Nature and strength of chalcogen- bonds

Bortoli, Marco; Ahmad, Shah Masood; Hamlin, Trevor A.; Bickelhaupt, F. Matthias; Orian, Laura

published in
Physical Chemistry Chemical Physics
2018

DOI (link to publisher)
10.1039/C8CP05922E

document version
Publisher's PDF, also known as Version of record

PCCP

PAPER

View Article Online
View Journal | View Issue

Cite this: *Phys. Chem. Chem. Phys.*, 2018, **20**, 27592

Nature and strength of chalcogen–π bonds†

Marco Bortoli,[a] Shah Masood Ahmad,[a] Trevor A. Hamlin,[b] F. Matthias Bickelhaupt*[bc] and Laura Orian*[a]

Received 20th September 2018,
Accepted 23rd October 2018

DOI: 10.1039/c8cp05922e

rsc.li/pccp

Chalcogen–π interactions occur between a covalently bound chalcogen atom that enters into a non-covalent interaction with an unsaturated moiety, a bonding motif found in various structures, such as, proteins. In this work, we have systematically explored and analyzed chalcogen–π interactions in model systems $\mathbf{X_2D}\cdots\mathbf{A}$ (with **D** = O, S, Se, Te; **X** = halogen; **A** = acetylene, ethylene and 2-butyne), using relativistic density functional theory (DFT). The nature and trends in stability of the chalcogen–π bonds are analyzed and interpreted in terms of quantitative MO theory in combination with a matching canonical energy decomposition analysis (EDA) scheme. We find that chalcogen–π bonds increase in strength as the X–D electronegativity difference becomes greater. Moreover, 2-butyne was found to participate in the strongest non-covalent interaction due to enhanced orbital interactions.

1 Introduction

"With courageous simplification, one might assert that the chemistry of the last century was largely the chemistry of covalent bonding, whereas that of the present century is more likely to be the chemistry of non-covalent binding."[1] This passage by Prof. Schneider appeared in a review on supramolecular chemistry and denotes how the role of non-covalent interactions is becoming more and more important in modern chemistry. Among these bonding mechanisms, which comprise also dipole–dipole, ion–dipole and π–π interactions, the most extensively studied is the hydrogen bond.[2] The classical scheme of the hydrogen bond, in which the H atom acts as an electron acceptor from an electronegative atom, has been applied also to other bonding motifs where the hydrogen atom is substituted by halogen, chalcogen, or pnicogen atoms to form halogen,[3–6] chalcogen,[7–16] and pnicogen bonds,[17–21] respectively. Recently, the chalcogen bond has received much attention due to the promising features making it amenable to application in many fields such as catalysis, ion transport and material and drug design.[22–28] In addition to that, a very recent survey of the PDB database showed that many protein–ligand complexes, in which the ligand contains a chalcogen atom, adopt structures that allow the formation of chalcogen bonds.[29] In this work, we focus our attention on a particular kind of bond acceptors, *i.e.* small organic molecules containing a double or triple bond. Our aim is to study and quantitatively analyze the behavior of the chalcogen–π bond. Investigation on these type of systems has found binding energies ranging between −3.3 and −6.6 kcal mol^{-1} with the main energetic contribution being assigned to a charge transfer from a π-orbital of the acceptor, localized around the C–C multiple bond, to the σ* antibonding orbital of the molecule containing the chalcogen.[30] Moreover, since evidence was found that the electronic environment could affect the strength of a chalcogen bond,[6,31] in this work we have focused our attention not only on the chalcogen or the substrate (which are directly taking part in the bond formation), but also on the atoms bonded to the chalcogen, to determine how the modification of the electronic environment around the bond could affect its strength. DFT calculations in combination with the activation strain analysis (ASA)[32] and energy decomposition analysis (EDA)[33] models were employed to quantitatively compute the strength of the chalcogen bond in a set of complexes of general formula $\mathbf{DX_2}\cdots\mathbf{A}$ in which **D** is the chalcogen bond donor (O, S, Se, or Te) **X** is a halogen and **A** is a small organic molecule containing an unsaturated bond (acetylene, ethylene and 2-butyne were selected for this study) that gives rise to an electron-rich π system. The three elements constituting the molecular complexes (**D**, **X**, and **A**) were systematically varied and all the possible permutations were investigated to accurately assess the effect each of them has on the stabilization deriving from the formation of a chalcogen bond.

2 Computational methodology

Density functional theory (DFT) calculations were carried out with the Amsterdam Density Functional (ADF) program.[34–36]

[a] *Dipartimento di Scienze Chimiche Università degli Studi di Padova, Via Marzolo 1, 35131 Padova, Italy. E-mail: laura.orian@unipd.it*
[b] *Department of Theoretical Chemistry and Amsterdam Center for Multiscale Modeling (ACMM), Vrije Universiteit Amsterdam, De Boelelaan 1083, 1081 HV Amsterdam, The Netherlands. E-mail: f.m.bickelhaupt@vu.nl*
[c] *Institute for Molecules and Materials (IMM), Radboud University, Heyendaalseweg 135, 6525 AJ Nijmegen, The Netherlands*

† Electronic supplementary information (ESI) available. See DOI: 10.1039/c8cp05922e

The geometries of the chalcogenides, unsaturated hydrocarbons, and the complexes were optimized imposing C_S symmetry. The functional BLYP[37,38] in combination with TZ2P basis was employed for all the elements. The TZ2P basis set is a large uncontracted set of Slater-type orbitals (STOs) of triple-ζ quality and has been augmented with two sets of polarization functions on each atom that is, 2p and 3d on H, 3d and 4f on C, S, F and Cl, 4d and 4f on Se and Br, and 5d and 4f on Te and I. The frozen-core approximation was adopted for the core electrons: up to 1s for C and F, up to 2p for S and Cl, up to 3p for Se and Br, and up to 4p for Te and I. An auxiliary set of s, p, d, f, and g STOs was used to fit the molecular density and to represent the Coulomb and exchange potentials accurately in each SCF cycle. Dispersion corrections were included employing the D3 scheme with the Becke–Johnson damping [D3(BJ)] developed by Grimme *et al.*[39] Scalar relativistic effects were accounted for through the zeroth-order regular approximation (ZORA).[40] This level of theory is referred to as ZORA-BLYP-D3(BJ)/TZ2P and was benchmarked and employed in theoretical studies of organochalcogenides.[41–43] Frequency calculations were employed to confirm the nature of the stationary points.

The activation strain analysis[32] was performed to quantitatively decompose the contributions to the chalcogen–π bonding energy in the complexes under investigation. The relative energy of a molecular complex can be written as the sum of strain contribution (ΔE_{strain}) and an interaction contribution (ΔE_{int}) eqn (1):

$$\Delta E = \Delta E_{strain} + \Delta E_{int} \quad (1)$$

ΔE_{strain} is the energy required for the geometrical deformation of the reacting species when they are brought from infinity to the geometry they acquire after complex formation and ΔE_{int} is the actual interaction energy between the fragments. This can be further divided, through energy decomposition analysis (EDA),[33] into the electrostatic interaction (ΔV_{elstat}), Pauli repulsion (ΔE_{Pauli}), and orbital interactions (ΔE_{oi}) contributions eqn (2):

$$\Delta E_{int} = \Delta V_{elstat} + \Delta E_{oi} + \Delta E_{Pauli} + \Delta E_{disp} \quad (2)$$

Since in the case of BLYP-D3(BJ) functional, an empirical correction to account for dispersion interaction is included, the term ΔE_{disp} is also added to eqn (2). To perform the ASA and the EDA single point energy calculations were run on the previously optimized geometries with a quadruple-ζ quality basis set. This level of theory is denoted as ZORA-BLYP-D3(BJ)/QZ4P//ZORA-BLYP-D3(BJ)/TZ2P.

The electron density distribution was analyzed using the Voronoi deformation density (VDD) method for computing fragment charges.[44,45] The Voronoi deformation density (VDD) method was chosen because it is basis set independent, unlike Mulliken charges, which are heavily dependent on basis choice.[45] The VDD method calculates the amount of electronic density that flows to or from a certain atom due to the bond formation, by spatial integration of the deformation density over the atomic Voronoi cell.

For selected cases, we have computed highly correlated *ab initio* reference data through CCSD(T) single-point calculations performed on ZORA-BLYP-D3(BJ)/TZ2P optimized geometries. In view of its accuracy and efficiency,[46] we chose the domain localized pair of natural orbitals coupled cluster with singles and double excitations treated explicitly and triple excitations treated perturbatively (DLPNO-CCSD(T)) as implemented in the Orca 4.0.0 software package.[47–49] Relativistic effects were accounted for through the second order scalar Douglas–Kroll–Hess method[50] and a quintuple ζ basis sets, designed for relativistic calculations, was employed. For the heaviest elements (Te and I) this basis set was not available in Orca. Therefore, for these two elements, the aug-cc-pVQZ-DK basis set was used instead of the quintuple-ζ basis. All the benchmark data are reported in the ESI† (Tables S1 and S2).

All energies were calculated with and without the counterpoise correction to account for the basis set superposition error (BSSE). Comparison between DFT and DLPNO-CCSD(T)/aug-cc-pV5Z level of theory for a selection of complexes resulted in a smaller average mean absolute error for the uncorrected energies (see ESI† for details), likely because of a fortuitous cancellation of this error in the uncorrected values.[51] Therefore, uncorrected energies are used throughout the paper.

3 Results and discussion

3.1 Geometrical parameters

The model systems have general formula $\mathbf{X_2D}\cdots\mathbf{A}$, in which **D** is a chalcogen bond donor atom (namely O, S, Se, or Te), **X** is a halogen atom, and **A** is an unsaturated organic molecule acting as chalcogen bond acceptor. In our study, 2-butyne (**2but**), acetylene (**ac**), and ethylene (**et**) were selected as model chalcogen bond acceptors. All $\mathbf{X_2D}\cdots\mathbf{A}$ combinations were optimized in the gas phase at the ZORA-BLYP-D3(BJ)/TZ2P using C_S symmetry. A representative set of optimized geometries (Fig. 1) displays the many similarities among the different complexes. Sulfur, selenium and tellurium compounds all display a chalcogen–π bond that is collinear to a halogen–chalcogen bond, adopting a T-like shape. Moreover, in these complexes the two chalcogen–halogen bonds show a slight length difference in favor of the one collinear to the chalcogen–π bond. Oxygen complexes show a slightly different structure because there is a rotation of the chalcogenide in the reflection plane. The resulting structure is Y shaped with almost equal chalcogen–halogen bonds. Donor–acceptor distances *d* (measured as the distance between the chalcogen atom and a carbon atom involved in the unsaturated bond) span a 0.62 Å range with $\mathbf{F_2O}\cdots$**2but** having the shortest distance, *i.e.* 2.59 Å, and $\mathbf{I_2Te}\cdots$**ac** showing the longest distance, *i.e.* 3.21 Å. These distances agree nicely with those of similar systems computed with high level *ab initio* methods.[30]

Voronoi deformation densities (VDDs) were calculated for the chalcogen atom in all the chalcogenides (Table 1). Since VDD charges do not represent an absolute charge value but only a relative flow of charge with respect to a reference structure,[45] their value cannot be absolutely related to the amount of charge on different atoms, but the comparison between the values for analogous atoms in two different complexes is useful to assess

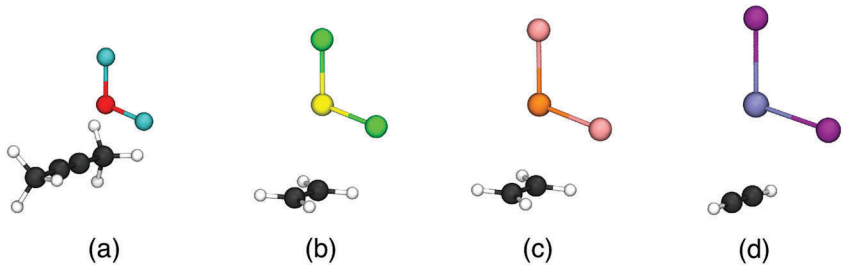

Fig. 1 Examples of the optimized structures of four complexes: **$F_2O\cdots$2but** (a), **$Cl_2S\cdots$et** (b), **$Br_2Se\cdots$et** (c) and **$I_2Te\cdots$ac** (d).

Table 1 Chalcogen–carbon distance (in Å) and Voronoi deformation densities (VDD, in a.u.) on chalcogen atom (D)[a]

Complex	d	VDD	Complex	d	VDD
$F_2O\cdots$ac	2.97	0.108	**$F_2Se\cdots$ac**	2.76	0.264
$Cl_2O\cdots$ac	3.10	−0.044	**$Cl_2Se\cdots$ac**	3.01	0.178
$Br_2O\cdots$ac	3.05	−0.097	**$Br_2Se\cdots$ac**	3.05	0.126
$I_2O\cdots$ac	3.08	−0.135	**$I_2Se\cdots$ac**	3.13	0.043
$F_2O\cdots$et	2.90	0.105	**$F_2Se\cdots$et**	2.68	0.272
$Cl_2O\cdots$et	2.98	−0.046	**$Cl_2Se\cdots$et**	2.94	0.181
$Br_2O\cdots$et	2.88	−0.098	**$Br_2Se\cdots$et**	2.97	0.128
$I_2O\cdots$et	2.93	−0.136	**$I_2Se\cdots$et**	3.06	0.044
$F_2O\cdots$2but	2.59	0.103	**$F_2Se\cdots$2but**	2.69	0.254
$Cl_2O\cdots$2but	2.78	−0.039	**$Cl_2Se\cdots$2but**	2.87	0.176
$Br_2O\cdots$2but	2.72	−0.089	**$Br_2Se\cdots$2but**	2.89	0.125
$I_2O\cdots$2but	2.83	−0.129	**$I_2Se\cdots$2but**	2.96	0.046
$F_2S\cdots$ac	2.93	0.193	**$F_2Te\cdots$ac**	2.83	0.287
$Cl_2S\cdots$ac	3.15	0.120	**$Cl_2Te\cdots$ac**	3.07	0.239
$Br_2S\cdots$ac	3.17	0.069	**$Br_2Te\cdots$ac**	3.12	0.201
$I_2S\cdots$ac	3.21	−0.003	**$I_2Te\cdots$ac**	3.21	0.123
$F_2S\cdots$et	2.86	0.195	**$F_2Te\cdots$et**	2.82	0.297
$Cl_2S\cdots$et	3.10	0.120	**$Cl_2Te\cdots$et**	3.00	0.244
$Br_2S\cdots$et	3.09	0.070	**$Br_2Te\cdots$et**	3.05	0.206
$I_2S\cdots$et	3.16	−0.004	**$I_2Te\cdots$et**	3.14	0.127
$F_2S\cdots$2but	2.77	0.189	**$F_2Te\cdots$2but**	2.81	0.264
$Cl_2S\cdots$2but	2.92	0.122	**$Cl_2Te\cdots$2but**	2.96	0.232
$Br_2S\cdots$2but	2.93	0.073	**$Br_2Te\cdots$2but**	3.00	0.197
$I_2S\cdots$2but	2.95	0.002	**$I_2Te\cdots$2but**	3.07	0.124

[a] Computed at ZORA-BLYP-D3(BJ)/QZ4P//ZORA-BLYP-D3(BJ)/TZ2P.

Table 2 Activation strain analysis (in kcal mol^{-1}) for the model systems[a]

Complex	ΔE	ΔE_{strain}	ΔE_{int}	Complex	ΔE	ΔE_{strain}	ΔE_{int}
$F_2O\cdots$ac	−1.3	0.2	−1.5	**$F_2Se\cdots$ac**	−7.5	0.8	−8.3
$Cl_2O\cdots$ac	−1.0	0.1	−1.1	**$Cl_2Se\cdots$ac**	−5.4	0.2	−5.6
$Br_2O\cdots$ac	−1.3	0.1	−1.4	**$Br_2Se\cdots$ac**	−5.0	0.2	−5.2
$I_2O\cdots$ac	−1.5	0.0	−1.5	**$I_2Se\cdots$ac**	−4.4	0.1	−4.5
$F_2O\cdots$et	−1.7	0.5	−2.2	**$F_2Se\cdots$et**	−9.1	1.6	−10.7
$Cl_2O\cdots$et	−1.6	0.2	−1.8	**$Cl_2Se\cdots$et**	−6.7	0.5	−7.2
$Br_2O\cdots$et	−2.2	0.2	−2.4	**$Br_2Se\cdots$et**	−6.4	0.4	−6.8
$I_2O\cdots$et	−2.4	0.1	−2.5	**$I_2Se\cdots$et**	−5.7	0.2	−5.9
$F_2O\cdots$2but	−3.9	2.6	−6.5	**$F_2Se\cdots$2but**	−11.4	2.0	−13.4
$Cl_2O\cdots$2but	−3.3	0.6	−3.9	**$Cl_2Se\cdots$2but**	−9.5	1.0	−10.5
$Br_2O\cdots$2but	−4.2	0.5	−4.7	**$Br_2Se\cdots$2but**	−9.3	0.7	−10.0
$I_2O\cdots$2but	−4.3	0.2	−4.5	**$I_2Se\cdots$2but**	−8.6	0.5	−9.1
$F_2S\cdots$ac	−4.3	0.3	−4.6	**$F_2Te\cdots$ac**	−9.4	1.2	−10.6
$Cl_2S\cdots$ac	−3.2	0.2	−3.4	**$Cl_2Te\cdots$ac**	−6.8	0.4	−7.2
$Br_2S\cdots$ac	−3.3	0.1	−3.4	**$Br_2Te\cdots$ac**	−6.2	0.3	−6.5
$I_2S\cdots$ac	−2.9	0.1	−3.0	**$I_2Te\cdots$ac**	−5.4	0.2	−5.6
$F_2S\cdots$et	−5.1	0.6	−5.7	**$F_2Te\cdots$et**	−11.7	2.0	−13.7
$Cl_2S\cdots$et	−4.0	0.3	−4.3	**$Cl_2Te\cdots$et**	−8.5	0.8	−9.3
$Br_2S\cdots$et	−4.1	0.2	−4.3	**$Br_2Te\cdots$et**	−7.9	0.6	−8.5
$I_2S\cdots$et	−3.9	0.1	−4.0	**$I_2Te\cdots$et**	−7.0	0.3	−7.3
$F_2S\cdots$2but	−7.3	1.3	−8.6	**$F_2Te\cdots$2but**	−13.2	2.4	−15.6
$Cl_2S\cdots$2but	−6.5	0.7	−7.2	**$Cl_2Te\cdots$2but**	−11.2	1.2	−12.4
$Br_2S\cdots$2but	−6.8	0.6	−7.4	**$Br_2Te\cdots$2but**	−10.7	0.9	−11.6
$I_2S\cdots$2but	−6.6	0.4	−7.0	**$I_2Te\cdots$2but**	−9.8	0.6	−10.4

[a] Computed at ZORA-BLYP-D3(BJ)/QZ4P//ZORA-BLYP-D3(BJ)/TZ2P.

which undergoes a greater electron density depletion or increase. Therefore, to calculate VDD charges independent of the chalcogen bond acceptor, all VDD charges were computed on the chalcogen atoms in the isolated chalcogenide molecules at the geometry they have in the final complex. Computed values identify a common trend that shows decreasing VDD charges as the chalcogen–halogen difference in electronegativity becomes less pronounced. For example, in the **$X_2Se\cdots$ac** series, VDD charges go from 0.264 to 0.043 a.u. when **X** changes from F to I and in the **$F_2D\cdots$ac** series from 0.287 to 0.108 a.u. as we ascend the group from Te to O.

3.2 Bonding analysis

Activation strain analyses (Table 2) and energy decomposition analyses (Table 3) were employed to quantify the different contributions that make up for the stabilization derived from the formation of the chalcogen bond. The interacting complexes were divided into two fragments, one consisting of the chalcogenide and the other of the unsaturated substrate. The effects on the bonding stabilization obtained with the modification of the chalcogen atom, of the accepting substrate, and of the halogen atoms were investigated, and data will be presented focusing on one component at a time in the three next paragraphs. In each of them, we will refer to ''series'' of compounds. A ''series'' consists of a set of compounds through which only **D**, **X**, or **A** is varied.

3.3 Chalcogen effect

Computed ΔE values show how the non-covalent interaction strength increases as the chalcogen becomes more electropositive. Consequently, complexes of tellurium show the highest stability whereas structures containing oxygen result in the least stabilized: for example, in the **$F_2D\cdots$ac** series the

Table 3 Energy decomposition analysis (in kcal mol^{-1}) of the model systems[a]

Complex	ΔE_{Pauli}	ΔV_{elstat}	ΔE_{oi}	ΔE_{disp}	Complex	ΔE_{Pauli}	ΔV_{elstat}	ΔE_{oi}	ΔE_{disp}
$F_2O\cdots ac$	4.5	−2.6	−2.4	−1.0	**$F_2Se\cdots ac$**	32.0	−18.9	−17.8	−3.6
$Cl_2O\cdots ac$	3.8	−1.6	−1.5	−1.0	**$Cl_2Se\cdots ac$**	16.5	−10.1	−8.2	−3.8
$Br_2O\cdots ac$	4.7	−1.9	−1.9	−2.3	**$Br_2Se\cdots ac$**	15.6	−9.3	−7.5	−4.0
$I_2O\cdots ac$	5.1	−1.9	−1.8	−2.9	**$I_2Se\cdots ac$**	13.0	−7.6	−5.7	−4.2
$F_2O\cdots et$	6.6	−3.4	−4.0	−1.4	**$F_2Se\cdots et$**	45.9	−25.7	−26.4	−4.5
$Cl_2O\cdots et$	6.4	−2.7	−3.0	−2.5	**$Cl_2Se\cdots et$**	23.7	−13.4	−12.4	−5.1
$Br_2O\cdots et$	8.6	−3.5	−4.2	−3.3	**$Br_2Se\cdots et$**	22.6	−12.6	−11.5	−5.3
$I_2O\cdots et$	8.8	−3.5	−3.8	−4.0	**$I_2Se\cdots et$**	18.9	−10.3	−9.0	−5.5
$F_2O\cdots 2but$	16.3	−8.4	−12.0	−2.4	**$F_2Se\cdots 2but$**	42.6	−26.5	−23.8	−5.7
$Cl_2O\cdots 2but$	10.5	−4.7	−5.8	−3.9	**$Cl_2Se\cdots 2but$**	28.1	−17.2	−14.6	−6.8
$Br_2O\cdots 2but$	12.9	−5.5	−7.2	−4.9	**$Br_2Se\cdots 2but$**	27.3	−16.4	−13.8	−7.2
$I_2O\cdots 2but$	11.8	−4.9	−5.4	−6.0	**$I_2Se\cdots 2but$**	23.7	−13.8	−11.1	−7.8
$F_2S\cdots ac$	15.4	−9.2	−8.0	−2.8	**$F_2Te\cdots ac$**	39.1	−23.7	−21.8	−4.2
$Cl_2S\cdots ac$	9.1	−5.3	−4.0	−3.2	**$Cl_2Te\cdots ac$**	21.4	−13.3	−10.8	−4.5
$Br_2S\cdots ac$	8.8	−5.0	−3.8	−3.4	**$Br_2Te\cdots ac$**	19.5	−12.0	−9.4	−4.6
$I_2S\cdots ac$	8.8	−4.7	−3.4	−3.7	**$I_2Te\cdots ac$**	16.0	−9.7	−7.2	−4.7
$F_2S\cdots et$	22.3	−12.3	−12.1	−3.6	**$F_2Te\cdots et$**	52.7	−30.7	−30.4	−5.3
$Cl_2S\cdots et$	12.6	−6.8	−5.9	−4.2	**$Cl_2Te\cdots et$**	30.9	−18.0	−16.3	−5.9
$Br_2S\cdots et$	13.5	−7.0	−6.3	−4.5	**$Br_2Te\cdots et$**	28.2	−16.2	−14.3	−6.2
$I_2S\cdots et$	12.2	−6.1	−5.3	−4.8	**$I_2Te\cdots et$**	23.4	−13.2	−11.2	−6.3
$F_2S\cdots 2but$	27.3	−16.3	−14.8	−4.8	**$F_2Te\cdots 2but$**	46.3	−30.2	−25.1	−6.6
$Cl_2S\cdots 2but$	19.5	−11.1	−9.6	−6.0	**$Cl_2Te\cdots 2but$**	32.4	−20.8	−16.3	−7.7
$Br_2S\cdots 2but$	19.8	−11.0	−9.7	−6.5	**$Br_2Te\cdots 2but$**	30.5	−19.3	−14.8	−8.0
$I_2S\cdots 2but$	20.3	−10.8	−9.0	−7.5	**$I_2Te\cdots 2but$**	27.0	−16.6	−12.3	−8.5

[a] Computed at ZORA-BLYP-D3(BJ)/QZ4P//ZORA-BLYP-D3(BJ)/TZ2P.

total stabilization increases from −1.3 kcal mol^{-1} for O to −4.3, −7.5 and −9.4 kcal mol^{-1} in the case of S, Se and Te respectively.

The main reason behind this trend is that an increasing interaction energy is computed when going from oxygen to tellurium complexes. Energy decomposition analysis shows that this increase in interaction stems from a more favorable contribution from ΔV_{elstat}, ΔE_{oi} and ΔE_{disp}. The enhanced electrostatic interaction originates from a more positive atomic charge when going from oxygen to tellurium: VDD charges on the chalcogen atom of 0.108, 0.193, 0.264 and 0.287 a.u. are computed for the four complexes of the **$F_2D\cdots ac$** series (Table 1). This is due to the increasing electropositivity of the chalcogen that results in a stronger shift of the charge density towards the halogen. The increased orbital interactions originate from a higher overlap between the frontier molecular orbitals of the two interacting fragments, namely, the HOMO of the unsaturated substrate and the LUMO of the chalcogenide (Table 4), which is the key orbital interaction in the formation of the chalcogen–π bond (Fig. 2). Taking again as an example the **$F_2D\cdots ac$** series, the HOMO–LUMO overlap goes from 0.06 in the case of oxygen to 0.13, 0.17 and 0.20 as we descend through the group to sulfur, selenium, and tellurium. These increasing overlap values reflect into ΔE_{oi} values: **$F_2O\cdots ac$** has the lowest contribution at −2.4 kcal mol^{-1} followed by sulfur selenium and tellurium at −8.0, −17.8 and −21.8 kcal mol^{-1}, respectively. Note that the trend of increasing HOMO–LUMO overlap S along the series, which enhances the orbital interactions ΔE_{oi}, dominates the trend of increasing HOMO–LUMO energy gap $\Delta\varepsilon$, which weakens the orbital interactions ΔE_{oi}. We recall that, in the framework of canonical molecular orbital theory, donor–acceptor orbital interactions are approximately proportional to $S^2/\Delta\varepsilon$.[52] Indeed, we find that this term increases from oxygen down to tellurium (Table 4).

Table 4 HOMO–LUMO gap $\Delta\varepsilon$ (in eV) and overlap S in selected model systems[a]

Complex	$\Delta\varepsilon$	S	$S^2/\Delta\varepsilon \times 10^3$
$F_2O\cdots ac$	1.84	0.06	1.95
$F_2S\cdots ac$	3.58	0.13	4.72
$F_2Se\cdots ac$	3.03	0.17	9.54
$F_2Te\cdots ac$	2.89	0.20	13.83
$Cl_2O\cdots ac$	2.01	0.06	1.79
$Cl_2S\cdots ac$	3.14	0.10	3.18
$Cl_2Se\cdots ac$	2.91	0.14	6.74
$Cl_2Te\cdots ac$	3.11	0.18	10.42
$Br_2O\cdots ac$	1.97	0.07	2.49
$Br_2S\cdots ac$	2.84	0.10	3.52
$Br_2Se\cdots ac$	2.75	0.13	6.14
$Br_2Te\cdots ac$	2.99	0.14	6.56
$I_2O\cdots ac$	2.14	0.07	2.29
$I_2S\cdots ac$	2.74	0.08	2.33
$I_2Se\cdots ac$	2.71	0.09	2.99
$I_2Te\cdots ac$	2.92	0.12	4.93

[a] Computed at ZORA-BLYP-D3(BJ)/QZ4P//ZORA-BLYP-D3(BJ)/TZ2P. For data on all model systems, see ESI.

Finally, dispersion contributions are computed to be higher for the heaviest chalcogens due to the harder nature of oxygen

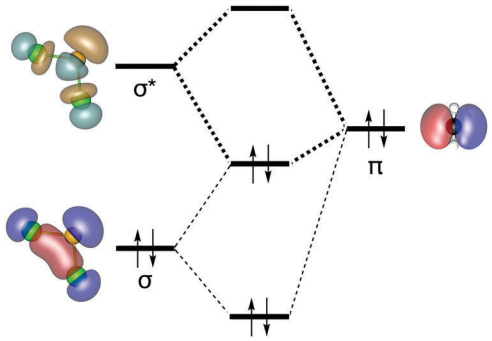

Fig. 2 Schematic frontier-orbital interaction diagram for chalcogen–π bonds (orbital isosurface: 0.04).

and sulfur, whose computed ΔE_{disp} are of −1.0 and −2.8 kcal mol^{-1} in the **F$_2$D**···**ac** series, and the increased polarizability of selenium and tellurium, whose dispersion contributions amount to −3.6 and −4.2 kcal mol^{-1} for **F$_2$Se**···**ac** and **F$_2$Te**···**ac**, respectively.

3.4 Substrate effect

Counterpart to the chalcogen bond donor, the unsaturated substrate acting as bond acceptor is very important in the determination of bond strength. Among our model systems, we computed that the highest stabilization is displayed in complexes of 2-butyne followed by ethylene and acetylene. Orbital interactions are one cause of this trend: they decrease from 2-butyne to ethylene to acetylene in most of the series (with the only exceptions of the **F$_2$Se**···**A** and **F$_2$Te**···**A** series) resulting in complexes that have a longer bond length. The decrease in orbital interactions is accompanied by a weaker electrostatic contribution which, for the three complexes in this series, is computed to be −17.2, −13.4 and −10.1 kcal mol^{-1}. This decrease in orbital and electrostatic terms leads to a systematic increase of the **D**···**A** distance as we pass from **2but** to **et** and finally **ac**. For example, it goes from 2.87 Å of **Cl$_2$Se**···**2but** to 2.94 Å of **Cl$_2$Se**···**et** and 3.01 Å of **Cl$_2$Se**···**ac** (Table 1).

In this case, the trend in $S^2/\Delta\varepsilon$ and thus in the orbital interactions ΔE_{oi}, along **2but**, **et**, and **ac**, is dominated by the trend in the HOMO–LUMO energy gap $\Delta\varepsilon$ (see Table 5). The overlap S varies only slightly. The HOMO–LUMO energy gap decreases along **ac**, **et**, and **2but** because along this series, the HOMO becomes increasingly destabilized and raises in energy. Such trends were also observed in similar chalcogen bonded complexes in which smaller HOMO–LUMO gaps were related to stronger bond formation.[9] The π bonding HOMO of **2but** is higher in energy than that of **et** because it is pushed up in energy by an antibonding combination with methyl C–H bonding orbitals (see Fig. 3). On the other hand, the π bonding HOMO of **ac** is lower in energy than that of **et** because of the shorter distance of a C–C triple bond which enhances the π overlap. In the **Cl$_2$Se**···**A** series, for example, this results in a HOMO–LUMO gap of 1.63, 2.39 and 3.03 eV for **2but**, **et** and **ac** respectively (Table 5), which translates into a ΔE_{oi} term of −14.6, −12.4 and −8.2 kcal mol^{-1} (Table 3).

Table 5 HOMO–LUMO energy gap $\Delta\varepsilon$ (in eV) and overlap S in selected model systems[a]

Complex	$\Delta\varepsilon$	S	$S^2/\Delta\varepsilon \times 10^3$
Cl$_2$O···**ac**	2.01	0.06	1.79
Cl$_2$O···**et**	1.51	0.07	3.24
Cl$_2$O···**2but**	0.58	0.06	6.17
Cl$_2$S···**ac**	3.14	0.10	3.18
Cl$_2$S···**et**	2.67	0.11	4.53
Cl$_2$S···**2but**	1.77	0.09	4.58
Cl$_2$Se···**ac**	2.91	0.14	6.74
Cl$_2$Se···**et**	2.40	0.15	9.37
Cl$_2$Se···**2but**	1.55	0.12	9.29
Cl$_2$Te···**ac**	3.11	0.18	10.42
Cl$_2$Te···**et**	2.57	0.20	15.57
Cl$_2$Te···**2but**	1.75	0.16	14.65

[a] Computed at ZORA-BLYP-D3(BJ)/QZ4P//ZORA-BLYP-D3(BJ)/TZ2P. For data on all model systems, see ESI.

Dispersion interactions are also more stabilizing for **2but** than for **et** or **ac** due to the size of the molecule which makes it more sensitive to van der Waals interactions. The variation in ΔE_{disp} is, however, more modest than that of electrostatic or orbital contributions. It changes, for example, from −6.8 kcal mol^{-1} for **Cl$_2$Se**···**2but** to −3.8 kcal mol^{-1} in the case of **Cl$_2$Se**···**ac** with the ethylene complex in the middle at −5.1 kcal mol^{-1}.

The decrease in orbital interactions going from **2but** to **et** and **ac** is reflected in the vibrational frequencies that we compute, using a harmonic approximation, for the chalcogen–π complexes. Our calculations show that the vibrational frequency associated with the stretching of the X–D bond collinear to the chalcogen–π bond decreases as we move from the isolated **X$_2$D** molecule to the **X$_2$D**···**A** complex (Table 6). The reason resides in the donor–acceptor orbital interaction in the chalcogen–π bond which leads to charge transfer into the LUMO of **X$_2$D**. This LUMO is a σ* X–D antibonding orbital; therefore, its population results in a weakening of the X–D bond and a lowering of the X–D stretch vibrational force constants and frequencies. The decrease of these frequencies becomes more pronounced as we go from **ac** to **et** to **2but** as further evidence that, along this series, the HOMO–LUMO interaction becomes stronger (*vide supra*).

3.5 Halogen effect

Modification of the halogens bonded to the chalcogen atom has a modest impact on the strength of the interaction. Nevertheless, throughout most of the analyzed series, a decrease in electrostatic and orbital interactions as the halogen becomes less electronegative results in a decrease in total stabilization of the chalcogen–π complex, thus making molecules containing fluorine the most stabilized, and those containing iodine the least stabilized. The strengthening of the bond by increasing the electronegativity of the group directly linked to the chalcogen bond donor was also previously observed in similar chalcogen bonded complexes.[9]

VDD charge calculation and orbital analysis show how the nature of the halogen directly affects the bond strength. In fact,

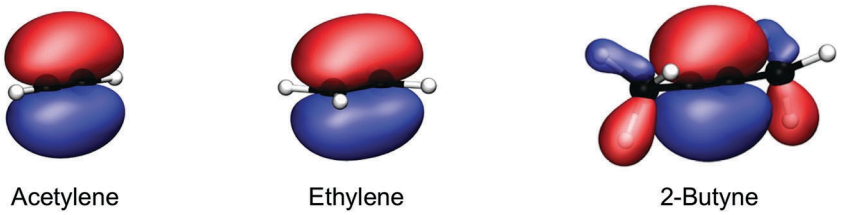

Fig. 3 HOMOs of the unsaturated substrates (orbital isosurface: 0.04).

Table 6 Stretching frequencies (in cm^{-1}) for the X–D bond collinear to the chalcogen bond in the isolated chalcogenides and in the π-bonded complexes

	X–D stretching frequency[a]						
		A					
X_2D	Isolated	ac		et		2but	
F_2O	763	712	(−51)	674	(−89)	563	(−200)
Cl_2O	539	521	(−18)	502	(−37)	447	(−92)
Br_2O	501	480	(−21)	458	(−43)	420	(−81)
I_2O	424	414	(−10)	402	(−22)	393	(−31)
F_2S	734	686	(−48)	667	(−67)	640	(−94)
Cl_2S	445	424	(−21)	415	(−30)	390	(−55)
Br_2S	360	340	(−20)	333	(−27)	314	(−46)
I_2S	312	294	(−18)	287	(−25)	275	(−37)
F_2Se	608	562	(−46)	543	(−65)	539	(−69)
Cl_2Se	355	339	(−16)	330	(−25)	322	(−33)
Br_2Se	261	250	(−11)	240	(−21)	241	(−20)
I_2Se	218	207	(−11)	200	(−18)	190	(−28)
F_2Te	575	534	(−41)	523	(−52)	520	(−55)
Cl_2Te	328	311	(−17)	303	(−25)	301	(−27)
Br_2Te	229	217	(−12)	211	(−18)	194	(−35)
I_2Te	182	174	(−8)	170	(−12)	166	(−16)

[a] The difference between the complexed and the isolated frequency is reported in parentheses.

Table 7 HOMO–LUMO gap Δε (in eV) and overlap S in selected model systems[a]

Complex	Δε	S	$S^2/\Delta\varepsilon \times 10^3$
$F_2S\cdots$**2but**	2.09	0.14	9.40
$Cl_2S\cdots$**2but**	1.77	0.09	4.58
$Br_2S\cdots$**2but**	1.49	0.08	4.30
$I_2S\cdots$**2but**	1.42	0.08	4.50
$F_2Se\cdots$**2but**	1.63	0.17	17.78
$Cl_2Se\cdots$**2but**	1.55	0.12	9.29
$Br_2Se\cdots$**2but**	1.41	0.11	8.59
$I_2Se\cdots$**2but**	1.40	0.08	4.58
$F_2Te\cdots$**2but**	1.55	0.18	20.96
$Cl_2Te\cdots$**2but**	1.75	0.16	14.65
$Br_2Te\cdots$**2but**	1.66	0.12	8.66
$I_2Te\cdots$**2but**	1.62	0.09	5.01

[a] Computed at ZORA-BLYP-D3(BJ)/QZ4P//ZORA-BLYP-D3(BJ)/TZ2P. For data on all model systems, see ESI.

the former confirms that the reduced electrostatic interaction derives from a decrease of the VDD charge on the chalcogen, when changing the substituent from fluorine to iodine, paralleled by an increase of the donor–acceptor distance (Table 1). For example, in the $X_2Se\cdots$**2but** series, VDD atomic charges are computed to be 0.254, 0.176, 0.125 and 0.046 a.u. and distances measure 2.69, 2.87, 2.89 and 2.96 Å passing from F to I. Bonding analysis reveals that $S^2/\Delta\varepsilon$ and thus ΔE_{oi} are dominated by the HOMO–LUMO overlap S. Thus, the chalcogenide's LUMO amplitude on the chalcogen atom and thus the overlap with the HOMO of the substrate decrease as the halogen goes from fluorine to iodine (*e.g.* from 0.17 in $F_2Se\cdots$**2but** to 0.08 in $I_2Se\cdots$**2but**, Table 7). The concomitant decrease in HOMO–LUMO gap Δε in these series is not strong enough to determine the trend in the $S^2/\Delta\varepsilon$ term which therefore decreases in complexes as we go to heavier halogens (Table 7). Thus, moving from F to I in the $X_2Se\cdots$**2but** series results in a weakening in ΔE_{oi} from −23.8 to −11.1 kcal mol^{-1}. This contributes to a weaker stabilization of complexes containing the least electronegative halogens such as in the $X_2Se\cdots$**2but** series where it is reduced from −11.4 kcal mol^{-1} in $F_2Se\cdots$**2but** to −8.6 kcal mol^{-1} in $I_2Se\cdots$**2but**. The few inconsistencies found, for example in the $F_2S\cdots$**2but** series, stem from very small ΔE_{oi} differences that are well below the 1 kcal mol^{-1} threshold and by the fact that on our analysis we focus only on the HOMO–LUMO interactions.

Thus, the $X_2D\cdots$**A** bond strength is governed by the difference in electronegativity between chalcogen (**D**) and halogen (**X**) as this determines the atomic charge and the amplitude of the X_2D LUMO on the chalcogen atom. This fits nicely with all main trends we compute: (i) the decreasing chalcogen bond strength as **X** becomes less electronegative along F, Cl, Br and I; and (ii) the increasing chalcogen bond strength as the chalcogen becomes more electropositive along O, S, Se and Te. Note that the oxygen complexes $X_2O\cdots$**A** are all relatively weakly bound with only minor and therefore less systematic variations in bond strength, *i.e.*, within a range of about 1 kcal mol^{-1}, along the various halogen substituents **X**.

Concerning the bond acceptor **A**, the presence of methyl groups (such as those in 2-butyne) is found to strengthen the chalcogen bond and therefore results in a weaker noncovalent interaction on going from **2but** to **et** and **ac**, as was previously observed in the literature.[9] Additionally, a stronger interaction of the bond donor with ethylene compared to acetylene is computed, in agreement with the results found in similar chalcogen bonded complexes[30] and also in analogous noncovalent interactions that involve P as the donor atom.[53]

4 Conclusions

In this work, a series of chalcogen–π bonded complexes was analyzed *in silico* to understand the physical factors that

determine the strength of the non-covalent interaction. Our calculations revealed that the stabilization of the complexes is enhanced when the difference in electronegativity between the chalcogen and the halogen substituents is greatest, going for example from **$I_2S\cdots$2but** to **$F_2S\cdots$2but** or from **$F_2O\cdots$2but** to **$F_2Te\cdots$2but**. Therefore, the complexes with the highest non-covalent interaction strength are those that contain the most electropositive chalcogen, *i.e.* tellurium, and the most electronegative halogen, *i.e.* fluorine. In addition, **2but** was seen to form the strongest chalcogen–π bond among the selected unsaturated substrates.

Molecular orbital analyses of the investigated **$X_2D\cdots A$** complexes reveal that the main cause of the strengthening of the bond is that an increase either in the chalcogen electropositivity or in the halogen substituent electronegativity clearly enhances the amplitude of the chalcogenide fragment's LUMO of the chalcogen atom and thus the orbital overlap with the HOMO of the unsaturated substrate resulting in an overall stronger chalcogen–π bond. Also, the different bond strengths computed for the various substrates are explained by orbital analyses, as differences mainly stem from the smaller HOMO–LUMO energy gap found in complexes of **2but**. Consequently, stronger orbital interactions result in complexes with shorter chalcogen–π bond distances and thus a more favorable $\Delta V_{\mathrm{elstat}}$ term which provides an additional stabilization in complexes with high chalcogen–halogen electronegativity differences and in those with 2-butyne.

Through a quantitative activation strain and energy decomposition analysis, the increase or decrease in bond strength was attributed directly to the intrinsic properties of the bond participants. Therefore, results from this study can be employed not only to describe the selected systems, but also to make predictions on the general behavior of the chalcogen–π interaction that can be extended to many other complexes. Moreover, they can be used to predict the strength of the chalcogen bonds in biological system based on the chemical nature of the atoms involved and may be exploited to create powerful designing tools for rationally designing and fine tuning novel molecular agents involving non-covalent interactions.

Conflicts of interest

There are no conflicts to declare.

Acknowledgements

M. B. is grateful to the University of Padua for financial support (PhD grant). Additionally, this work was supported by the Netherlands Organization for Scientific Research (NWO).

References

1 H. J. Schneider, *Angew. Chem., Int. Ed.*, 2009, **48**, 3924–3977.
2 G. Gilli and P. Gilli, *The Nature of the Hydrogen Bond*, Oxford University Press, Oxford, UK, 2009.
3 P. Politzer, P. Lane, M. C. Concha, Y. Ma and J. S. Murray, *J. Mol. Model.*, 2007, **13**, 305–311.
4 P. Auffinger, F. A. Hays, E. Westhof and P. S. Ho, *Proc. Natl. Acad. Sci. U. S. A.*, 2004, **101**, 16789–16794.
5 P. Politzer, J. S. Murray and T. Clark, *Phys. Chem. Chem. Phys.*, 2013, **15**, 11178–11189.
6 S. A. C. McDowell and A. D. Buckingham, *ChemPhysChem*, 2018, **19**, 1756–1765.
7 W. Wang, B. Ji and Y. Zhang, *J. Phys. Chem. A*, 2009, **113**, 8132–8135.
8 D. J. Pascoe, K. B. Ling and S. L. Cockroft, *J. Am. Chem. Soc.*, 2017, **139**, 15160–15167.
9 V. Oliveira, D. Cremer and E. Kraka, *J. Phys. Chem. A*, 2017, **121**, 6845–6862.
10 U. Adhikari and S. Scheiner, *J. Phys. Chem. A*, 2014, **118**, 3183–3192.
11 L. M. Azofra, I. Alkorta and S. Scheiner, *Phys. Chem. Chem. Phys.*, 2014, **16**, 18974–18981.
12 L. M. Azofra and S. Scheiner, *J. Phys. Chem. A*, 2014, **118**, 3835–3845.
13 R. Sedlak, S. M. Eyrilmez, P. Hobza and D. Nachtigallova, *Phys. Chem. Chem. Phys.*, 2018, **20**, 299–306.
14 R. Shukla and D. Chopra, *Phys. Chem. Chem. Phys.*, 2016, **18**, 13820–13829.
15 R. Shukla and D. Chopra, *J. Chem. Sci.*, 2016, **128**, 1589–1596.
16 F. De Vleeschouwer, M. Denayer, B. Pinter, P. Geerlings and F. De Proft, *J. Comput. Chem.*, 2018, **39**, 557–572.
17 V. Oliveira and E. Kraka, *J. Phys. Chem. A*, 2017, **121**, 9544–9556.
18 A. Bauzá, D. Quiñonero, P. M. Deyà and A. Frontera, *CrystEngComm*, 2013, **15**, 3137–3144.
19 K. T. Mahmudov, M. N. Kopylovich, M. F. C. Guedes da Silva and A. J. L. Pombeiro, *Coord. Chem. Rev.*, 2017, **345**, 54–72.
20 G. Sánchez-Sanz, I. Alkorta, C. Trujillo and J. Elguero, *ChemPhysChem*, 2013, **14**, 1656–1665.
21 G. Sánchez-Sanz, C. Trujillo, I. Alkorta and J. Elguero, *Phys. Chem. Chem. Phys.*, 2016, **18**, 9148–9160.
22 S. Benz, J. López-Andarias, J. Mareda, N. Sakai and S. Matile, *Angew. Chem., Int. Ed.*, 2017, **56**, 812–815.
23 S. Benz, M. Macchione, Q. Verolet, J. Mareda, N. Sakai and S. Matile, *J. Am. Chem. Soc.*, 2016, **138**, 9093–9096.
24 K. T. Mahmudov, M. N. Kopylovich, M. F. C. Guedes da Silva and A. J. L. Pombeiro, *Dalton Trans.*, 2017, **46**, 10121–10138.
25 B. R. Beno, K. S. Yeung, M. D. Bartberger, L. D. Pennington and N. A. Meanwell, *J. Med. Chem.*, 2015, **58**, 4383–4438.
26 L. Orian and S. Toppo, *Free Radical Biol. Med.*, 2014, **66**, 65–74.
27 L. P. Wolters and L. Orian, *Curr. Org. Chem.*, 2015, **20**, 189–197.
28 M. Dalla Tiezza, G. Ribaudo and L. Orian, *Curr. Org. Chem.*, 2018, DOI: 10.2174/1385272822666180803123137.
29 K. Kříž, J. Fanfrlík and M. Lepšík, *ChemPhysChem*, 2018, **19**, 2540–2548.
30 V. d. P. N. Nziko and S. Scheiner, *J. Phys. Chem. A*, 2014, **118**, 10849–10856.

31 M. D. Esrafili and M. Vakili, *Mol. Phys.*, 2014, **112**, 2746–2752.
32 F. M. Bickelhaupt and K. N. Houk, *Angew. Chem., Int. Ed.*, 2017, **56**, 10070–10086.
33 F. M. Bickelhaupt and E. J. Baerends, in *Reviews in Computational Chemistry*, ed. K. B. Lipkowitz and D. B. Boyd, John Wiley & Sons, Inc., New York, 2000, vol. 73, pp. 1–86.
34 G. te Velde, F. M. Bickelhaupt, E. J. Baerends, C. Fonseca Guerra, S. J. A. van Gisbergen, J. G. Snijders and T. Ziegler, *J. Comput. Chem.*, 2001, **22**, 931–967.
35 C. Fonseca Guerra, J. G. Snijders, G. te Velde and E. J. Baerends, *Theor. Chem. Acc.*, 1998, **99**, 391–403.
36 E. J. Baerends, T. Ziegler, A. J. Atkins, J. Autschbach, D. Bashford, A. Bérces, F. M. Bickelhaupt, C. Bo, P. M. Boerritger, L. Cavallo, D. P. Chong, D. V. Chulhai, L. Deng, R. M. Dickson, J. M. Dieterich, D. E. Ellis, M. van Faassen, A. Ghysels, A. Giammona, S. J. A. van Gisbergen, A. W. Götz, S. Gusarov, F. E. Harris, P. van den Hoek, C. R. Jacob, H. Jacobsen, L. Jensen, J. W. Kaminski, G. van Kessel, F. Kootstra, A. Kovalenko, M. Krykunov, E. van Lenthe, D. A. McCormack, A. Michalak, M. Mitoraj, S. M. Morton, J. Neugebauer, V. P. Nicu, L. Noodleman, V. P. Osinga, S. Patchkovskii, M. Pavanello, C. A. Peeples, P. H. T. Philipsen, D. Post, C. C. Pye, W. Ravenek, J. I. Rodríguez, P. Ros, R. Rüger, P. R. T. Schipper, H. van Schoot, G. Schreckenbach, J. S. Seldenthuis, M. Seth, J. G. Snijders, M. Solà, M. Swart, D. Swerhone, G. te Velde, P. Vernooijs, L. Versluis, L. Visscher, O. Visser, F. Wang, T. A. Wesolowski, E. M. van Wezenbeek, G. Wiesenekker, S. K. Wolff, T. K. Woo and A. L. Yakovlev, *ADF 2016, SCM, Theoretical Chemistry*, Vrije Universiteit, Amsterdam, The Netherlands, 2016.
37 A. D. Becke, *Phys. Rev. A: At., Mol., Opt. Phys.*, 1988, **38**, 3098–3100.
38 C. Lee, W. Yang and R. G. Parr, *Phys. Rev. B: Condens. Matter Mater. Phys.*, 1988, **37**, 785–789.
39 S. Grimme, S. Ehrlich and L. Goerigk, *J. Comput. Chem.*, 2011, **32**, 1456–1465.
40 E. van Lenthe, E. J. Baerends and J. G. Snijders, *J. Chem. Phys.*, 1994, **101**, 9783–9792.
41 F. Zaccaria, L. P. Wolters, C. Fonseca Guerra and L. Orian, *J. Comput. Chem.*, 2016, **37**, 1672–1680.
42 M. Bortoli, M. Torsello, F. M. Bickelhaupt and L. Orian, *ChemPhysChem*, 2017, **18**, 2990–2998.
43 M. Bortoli, F. Zaccaria, M. Dalla Tiezza, M. Bruschi, C. Fonseca Guerra, F. M. Bickelhaupt and L. Orian, *Phys. Chem. Chem. Phys.*, 2018, **20**, 20874–20885.
44 F. L. Hirshfeld, *Theor. Chim. Acta*, 1977, **44**, 129–138.
45 C. Fonseca Guerra, J. W. Handgraaf, E. J. Baerends and F. M. Bickelhaupt, *J. Comput. Chem.*, 2004, **25**, 189–210.
46 C. Riplinger and F. Neese, *J. Chem. Phys.*, 2013, **138**, 034106.
47 F. Neese, *WIREs Comput. Mol. Sci.*, 2012, **2**, 73–78.
48 C. Riplinger, B. Sandhoefer, A. Hansen and F. Neese, *J. Chem. Phys.*, 2013, **139**, 134101.
49 C. Riplinger, P. Pinski, U. Becker, E. F. Valeev and F. Neese, *J. Chem. Phys.*, 2016, **144**, 024109.
50 M. Reiher, *WIREs Comput. Mol. Sci.*, 2012, **2**, 139–149.
51 Ł. M. Mentel and E. J. Baerends, *J. Chem. Theory Comput.*, 2014, **10**, 252–267.
52 T. A. Albright, J. K. Burdett and M. H. Whangbo, *Orbital Interactions in Chemistry*, John Wiley & Sons, Inc., Hoboken, NJ, USA, 2nd edn, 2013.
53 S. Scheiner and U. Adhikari, *J. Phys. Chem. A*, 2011, **115**, 11101–11110.